Chemical Engineering Research and Design 228 (2026) 621–634

Contents lists available at ScienceDirect

Chemical Engineering Research and Design

journal homepage: www.elsevier.com/locate/cherd

A comprehensive methodology for parameter assessment in solid-state fermentation modelling

Anna Carrasco-García [1], Albert Guisasola [2], Javier Moral-Vico [1,*], Teresa Gea [1]

Department of Chemical, Biological and Environmental Engineering, Escola d'Enginyeria, Universitat Autònoma de Barcelona, Barcelona, Spain

ARTICLE INFO

Keywords:
Solid-state fermentation
Process modelling
Metabolic yield
Kinetics

ABSTRACT

Solid-state fermentation (SSF) is a promising technology for bioproduct generation within a circular bioeconomy framework, but its commercial application remains limited by heat and mass transfer constraints. In this study, we present a comprehensive experimental methodology for estimating key parameters required for modelling SSF processes. The objective of this study is to establish an experimental methodology for determining model parameters and, through a sensitivity analysis, evaluate their influence on the validation of a mathematical model for SSF processes. Using sophorolipid (SL) production by *Starmerella bombicola* as a case study, we determine thermal properties, kinetic parameters, and transfer coefficients, and validate them through temperature profile simulations in a 22-L bioreactor. The experimentally determined values were: specific heat capacity of 1.55 J g^{-1} $°C^{-1}$, thermal conductivity of 0.127 W m^{-1} $°C^{-1}$, heat transfer coefficient of 9790 ± 2.25 W m^{-3} $°C^{-1}$, mass transfer coefficient 0.00189 ± 0.00078 s^{-1}, metabolic heat yield of 1.34 × 10^7 J kg^{-1} biomass and a specific growth rate of 0.389 h^{-1}. A sensitivity analysis identifies microbial growth kinetics and heat yield as the most critical parameters influencing model accuracy, while thermal and transport parameters show low sensitivity. This integrated approach provides both a robust modelling framework and specific values applicable to SSF-based SL production, supporting scale-up efforts and adaptation to other solid matrices or microbial systems.

1. Introduction

Solid-state fermentation (SSF) involves growing microorganisms on a moist, porous matrix composed of substrates, nutrients, and a support material, which can be either inert or a substrate itself. The matrix contains enough water to support microbial growth, but there is no free-flowing water. During fermentation, microorganisms consume the substrates along with the oxygen supplied to the reactor, to produce the desired bioproduct, as well as CO_2, water, and metabolic heat (Raghavarao et al., 2003; Finkler et al., 2021). SSF enables the production of diverse bioproducts such as enzymes, biopesticides, or biosurfactants, using a variety of substrates with diverse characteristics including lignocellulosic residues and oil cakes (Kumar et al., 2021; Sánchez et al., 2024). Due to its ability to valorise solid waste and biomass, SSF has great potential to support the transition towards a circular bioeconomy. A defining characteristic of SSF is the use of low-cost, renewable materials, predominantly agro-industrial residues, as substrates or structural support (Arora et al., 2018; Hamidi-Esfahani et al., 2004; Casciatori et al., 2016). This strategy not only mitigates the environmental footprint associated with waste accumulation but also enables the recovery of value-added products from materials that would otherwise be discarded. Consequently, SSF contributes to more sustainable bioprocessing by aligning waste valorisation with resource efficiency.

However, several significant challenges need to be addressed for the full implementation of SSF at a commercial scale (Raghavarao et al., 2003; Kumar et al., 2021; Arora et al., 2018). The three-phase heterogeneity, solid compactness, and low thermal conductivity of the organic matrix contribute to metabolic heat accumulation, further raising the process temperature. This uncontrolled temperature rise can i) deactivate or kill the microorganisms, thus decreasing productivity, ii) denature the target bioproduct or iii) dry out the solids due to water evaporation. A decrease in the moisture content of the solid hinders nutrient absorption and diffusion (Sánchez et al., 2024; Hamidi-Esfahani

* Corresponding author.
E-mail address: antoniojavier.moral@uab.cat (J. Moral-Vico).
[1] Composting Research Group (GICOM)
[2] GENOCOV

https://doi.org/10.1016/j.cherd.2026.03.024
Received 26 June 2025; Received in revised form 12 March 2026; Accepted 13 March 2026
Available online 20 March 2026

et al., 2004). In addition, water plays a crucial role in fermentation, not only by facilitating microbial growth and metabolic activity but also by contributing to the cooling process through evaporation. Thus, maintaining appropriate moisture levels is essential for the success of the SSF process.

Effective control of the SSF process requires robust engineering capabilities to manage heat transfer within the reactor. In this context, mathematical modelling is being employed as a valuable tool to predict process performance, paying special attention to the evolution of temperature and moisture based on energy and mass balances. Beyond prediction, such models also support decision-making by enabling the optimisation of bioreactor design and operation, as well as the assessment of aeration strategies in terms of their effects and energy costs, thereby providing a basis for evaluating the sustainability of the process. In addition, they provide a cost-effective means of rapidly evaluating design and operational strategies, allowing the rapid identification of strategies with the greatest potential to mitigate overheating, without relying solely on large-scale experimental trials (Ashley et al., 1999).

Despite growing interest, only a few studies have developed SSF models. One of the most complete approaches is that of Casciatori et al., (Casciatori et al., 2016), who implemented a two-phase and two-dimensional mathematical model to describe the heat and mass transfer in a SSF system with one single substrate (Casciatori et al., 2016). A comprehensive mathematical model of an SSF bioreactor typically requires two sub-models, one describing the growth kinetics of the microorganism and the other describing the energy and mass balances, as well as transport phenomena (Kumar et al., 2021; Arora et al., 2018; Mitchell, 2006). The level of detail in each sub-model is determined by the simplifications and assumptions applied during model development. Such models rely on multiple system-specific input values, including physico-chemical properties of the solids, transport coefficients, and microbial growth parameters. Machine learning (ML) approaches are increasingly relevant in bioprocesses, as they can compile experimental data and transform it into predictive models. In SSF, ML has so far been applied primarily to support experimental decision-making. For example, ML was used to analyse data from 410 Maotai-flavor Baijiu samples, enabling the classification of diverse base types and improving blending efficiency and quality control (Yang et al., 2025). In another application, ML was employed to model, predict, and optimize the combination and concentration of surfactants and metabolic inducers within a predefined multi-substrate blend, with the aim of maximizing lipase production (Amenaghawon et al., 2024). Despite these advances, ML has not yet been applied in SSF to predict mass or energy transfer within the solid matrix during the fermentation process.

Beyond the complexity of the mathematical modeling itself, an additional limitation in SSF modeling is the lack of standardized methodologies for determining key parameters (Mitchell et al., 2023), such as thermal properties of the solids. As previously mentioned, ineffective heat transfer in SSF is primarily due to the poor thermal conductivity of the solids (Casciatori et al., 2013; Zhang et al., 2017; Casciatori et al., 2014). The value of thermal conductivity largely depends on the composition of the solids, the moisture content, and the porosity of the solid structure. For this reason, several studies have focused on measuring thermal conductivity at different moisture levels and porosities to establish reliable correlations (Casciatori et al., 2013; Zhang et al., 2017). In addition to thermal conductivity, the specific heat capacity of the solid is a relevant parameter, which is directly related to the accumulation of energy within the solid phase during fermentation and plays a key role in understanding the thermal dynamics of the process.

Transport coefficients, such as those for mass and heat transfer, also require careful estimation. Various approaches have been reported for this purpose. Von Meien and Mitchell, utilized empirical equations derived from experimental studies on the drying of corn (Von Meien and Mitchell, 2002). Alternatively, Casciatori et al., (Casciatori et al., 2016) used a theoretical approach based on dimensionless numbers. In this case, the Nusselt number was used to estimate the heat transfer coefficient, while the Sherwood number was employed for the mass transfer coefficient. An alternative method estimated transfer coefficients using drying, cooling and heating experiments on an abiotic fermentation bed. Based on a two-phase model and experimental data, the coefficients were estimated. The approach focused on validating the model's accuracy when predicting temperature evolution within the bed (Finkler et al., 2021).

Another critical parameter is the specific growth rate, which influences metabolic heat production and is also strongly affected by temperature and moisture content (Hamidi-Esfahani et al., 2004; Maddikeri et al., 2015). While calculating this rate from biomass data is conceptually simple, biomass quantification in fermented solids remains a challenge due to system heterogeneity and biomass penetration into the substrate. Common methods involve measuring microbial components like glucosamine, ergosterol, or enzyme activity but these are time-consuming and impractical for real-time monitoring, limiting their application for process control (Hamidi-Esfahani et al., 2004; Scotti et al., 2001; Abd-Aziz et al., 2008; Nout et al., 1987; Rodríguez-Rodríguez et al., 2010; Feng et al., 2005; Córdova-López et al., 1996; Favela-Torres et al., 1998). Alternatively, indirect methods such as monitoring oxygen consumption, CO_2 production, or metabolic heat offer real-time process insights, allowing operational adjustments. Moreover, correlating these indirect indicators with actual biomass concentration is not straightforward. Although these do not cover the high diversity of solid matrices composition based on non-lignocellulosic wastes. Therefore, to accurately apply mass and energy balances, it is crucial to know all relevant parameters specific to the mathematical models. Additionally, there is no clear consensus on how to calculate all required parameters or how to incorporate them into comprehensive SSF models.

To address these challenges, the present study proposes a comprehensive methodology for determining and integrating critical parameters into SSF models. The main objective is to provide a comprehensive experimental framework for parameter estimation, enabling the implementation of a mathematical model for an SSF system. An additional goal is to report the resulting values of these parameters and coefficients for the specific case of sophorolipid (SL) production from sunflower oil cake, and to evaluate, through a sensitivity analysis, their influence on the validation of a mathematical model for SSF.

For this, we build upon previous research on glycolipid biosurfactant production (Rodríguez et al., 2021; Oiza et al., 2024; Eras-Muñoz et al., 2024). Specifically, the system focuses on the production of sophorolipids (SLs) using the well-known yeast *Starmerella bombicola*, with a solid matrix composed of sunflower oil cake as a hydrophobic carbon source, glucose as a hydrophilic carbon source, yeast extract and urea as nitrogen sources, and wheat straw as an inert support. The diacetylated lactonic C18:1 congener is consistently reported as the predominant SL. This SSF system has been operated at laboratory scale and scaled up to 22-L and 100-L bioreactors, where the aforementioned challenges have been encountered (Rodríguez et al., 2021). The production of Bacillus thuringiensis (Bt)-derived biopesticides at a 100-L scale was successfully implemented (Mejias et al., 2025). However, at this and larger scales, it becomes necessary to introduce higher aeration rates or alternative cooling mechanisms, since the capacity for heat dissipation through the bioreactor walls decreases as the reactor diameter increases. For instance, Pilot et al., (Pitol et al., 2016) regulated air temperature to effectively control heat accumulation and optimize enzyme activity in a 200-L SSF system. However, to the best of our knowledge, there are no reports describing the operation of packed-bed SSF systems at industrial scale (in the order of m^3). This lack of information highlights the importance of developing robust process models to guide scale-up and predict performance under large-scale conditions.

The parameters estimated in this study will be validated using the mass and energy balance equations proposed by Casciatori et al., (Casciatori et al., 2016) and a sensitivity analysis will be undertaken as well (Casciatori et al., 2016). The mathematical model employed in this

study is based on the one proposed by Casciatori et al (Casciatori et al., 2016)., with two key modifications: the inclusion of basal metabolic heat in the solid-phase energy balance, and the incorporation of solid concentration as a function of the two main substrates, biomass and product. In addition, the estimated values of all key parameters and transfer coefficients are reported for this SSF system, providing a useful reference for future modelling efforts. Finally, the methodology proposed herein is intended to be adaptable to other SSF systems involving different substrates, microorganisms, and targeted bioproducts.

2. Materials and methods

2.1. Materials

The winterization sunflower oil cake (WOC) was provided by the oil refinery LIPSA (Lípidos Santiga S.A., Barcelona, Spain). The wheat straw was provided by the veterinary department of the UAB (Universitat Autònoma de Barcelona). D-(+)-Glucose (99.5%), urea (99.0%), cyclohexane HPLC (99.9%), methanol HPLC (99.9%), absolute ethanol HPLC, acetonitrile HPLC (99.9%), formic acid HPLC, potassium hydroxide (85%), glycerol (99.5%) and ergosterol (95%) were all purchased from Sigma-Aldrich (Barcelona, Spain). Soy peptone and agar-agar powder for bacteriology were purchased from Scharlab. Yeast extract and malt extract were purchased from Fisher BioReagents.

2.2. Yeast strain and inoculum preparation

Starmerella Bombicola ATCC 22214 was obtained from the American Type Culture Collection (Manassas, USA). The microorganism was conserved as glycerol stocks at −80 ºC. The strain was grown for 48 h at 30 ºC on agar streak plates containing (g L^{-1}): 10 of dextrose; 5 of peptone; 3 of malt extract, 3 of yeast extract; and 20 of agar. Then, with the support of a loop full, the microorganism was transferred from the agar streak plate into a 500 mL Erlenmeyer flask with 100 mL of sterile medium. The composition of the medium was: 10 g L^{-1} of dextrose, 10 g L^{-1} of peptone, 5 g L^{-1} of malt extract and 3 g L^{-1} of yeast extract. In addition, 10 g L^{-1} of glucose was also added. Immediately, the culture was incubated in an orbital incubator shaker at 30 ºC, 180 rpm for 48 h.

2.3. Solid-state fermentation

SSF experiments were conducted to validate the mathematical model and to estimate key model parameters, including microbial kinetics and the yield of biomass production related to glucose consumption, as well as SL production related to the fat consumption. The solid matrix composition was divided into the glucose as hydrophilic carbon source (0.11 g g^{-1} total), the WOC as hydrophobic carbon source (0.52 g g^{-1} total), urea (0.0011 g g^{-1} total) and yeast extract (0.011 g g^{-1} total) as nitrogen and nutrients sources and the wheat straw as solid support (0.36 g g^{-1} total), all values in dry basis. The moisture content was adjusted to 75% of water holding capacity (WHC) of the wheat straw (2.93 g water g^{-1} wheat straw) in all experiments. The solid matrix and the aqueous solution were separately autoclaved at 121 ºC for 20 min.

Solid-state fermentation experiments were carried out in self-made 0.5 L cylindrical polyvinylchloride packed-bed bioreactor, with a total weight mass of 68.67 g, operated in thermostatic baths at 30 ºC, as previously described in literature (Eras-Muñoz et al., 2024; Jiménez-Peñalver et al., 2016). Under sterile conditions, the solid and aqueous solution were mixed and inoculated with 6.4 mL of *S. bombicola.* Humidified air was supplied from the bottom at a flow rate of 30 mL min^{-1} using a mass flow controller (Bronkhorst, Spain) unless otherwise indicated. The exhaust air exited the reactor from the top, passed through an Erlenmeyer flask used as a water trap, and reached an oxygen sensor (Alphasense, UK) to monitor oxygen content. The solid-state fermentation process was monitored for 11 days to evaluate the yield of biomass production related to glucose consumption and SL production related to the fat consumption. For this purpose, nine 0.5 L packed-bed reactors were prepared, with one reactor sacrificed at each sampling point to analyse specific parameters at days 0, 1, 2, 3, 4, 5, 6, 7, and 11. The parameters measured included colony-forming unit (CFU), pH, and moisture, glucose, fat, and SL crude.

On the other hand, the experiments for the validation of the mathematical model based on the obtained parameters were carried out in a 22-L bench-scale packed-bed bioreactor. This bioreactor consisted of a cylindrical stainless-steel equipped with a perforated plate at the bottom part to separate the solid matrix from the distribution of humidified air. Detailed operating conditions are available in our previous work (Rodríguez et al., 2021). The solid fermentation matrix had a total mass of 2713 g, and was inoculated with 0.279 L of *S. bombicola* for a total 2992 g. The oxygen concentration in the exhaust gases was on-line monitored and used to calculate the oxygen uptake-rate (OUR) and the cumulative oxygen consumption (COC). Furthermore, temperature sensors (standard Thermochron iButton device, Maxim Integrated, U.S.) were placed in three axial positions and three radial positions of the reactor to monitor the evolution during the fermentation process. Room temperature (Fig. S1 in supplementary material) was continuously measured throughout the experiment, as it varied over time due to changing weather conditions. This time-dependent profile was incorporated in the simulations instead of assuming a constant value. Temperature peaks were observed during periods when the reactor was exposed to direct sunlight in the afternoon during the experiment.

2.4. Extraction and quantification of sophorolipids

Crude SL extraction was obtained through solid-liquid extractions in duplicate using ethyl acetate as solvent (Eras-Muñoz et al., 2024; Jiménez-Peñalver et al., 2016; Rodríguez et al., 2021). Briefly, 10 g of crushed fermented solid were mixed with 100 mL of ethyl acetate (1:10, w v^{-1}) using an orbital shaker at 200 rpm, 25 °C for 1 h. Subsequently, anhydrous sodium sulfate was added to remove residual moisture from the extract. Solvent extractions were filtered through a Whatman filter paper Grade 1 and concentrated by rotary evaporation under vacuum at 40 °C and 20 rpm. The crude SL obtained after solvent evaporation was washed with 40 mL of *n*-hexane (1:4 w v^{-1}) to remove any oily residue such as fatty acids from the fermentation process. Finally, the crude SL samples were stored at 4 °C for further analysis such as SLs mix quantification.

2.5. Physicochemical parameters of the solid

2.5.1. Heat capacity of the solid

The heat capacity of the solid was estimated using a differential scanning calorimeter (DSC 823e, Mettler Toledo). The samples were crushed in order to minimise sample heterogeneity and left to dry at 100 ºC for 24 h. Next, the samples were left to dry at 100 ºC for 24 h. Then, the sample was weighed in an aluminium crucible and sealed with aluminium lid. The DSC equipment was purged with dry nitrogen at a flow rate of 10–5 mL min^{-1} throughout the analysis. The sapphire standard measurement method involves performing isothermal holds before and after the temperature ramp of interest. Specifically, the first isothermal step was conducted at −15 ºC for 10 min, followed by a heating ramp from 15 ºC to 80 ºC with a rate of 10 ºC min^{-1}, and a final isothermal hold at 80 ºC for 10 min. The equation applied to calculate the specific heat capacity was the following:

$$Cp = \left(\frac{HF_{Sample}}{HF_{Sapphire}}\right) \times \left(\frac{M_{Sapphire}}{M_{Sample}}\right) \times Cp_{Sapphire} \quad (1)$$

Where HFSample is the heat flow of the sample (mW), HFSapphire is the heat flow of the blank (mW), MSapphire is the mass of the blank (mg), MSample is the mass of the sample (mg) and CpSapphire is the specific heat capacity of the blank (J g^{-1} ºC^{-1}). The resulting specific heat

capacity was obtained as a function of temperature in the range of 25 °C to 75 °C.

2.5.2. Thermal conductivity of the solid

The thermal conductivity was determined using a thermal properties analyser (Isomet 2114 Applied Precision). The thermal analyser was connected to a needle probe which must penetrate the sample to ensure complete contact. A total of three measurements were performed.

2.6. Calorimetry

Calorimetry experiments were designed to quantify metabolic heat production. These experiments were conducted in a 0.5 L Dewar® vessel (KGW Isotherm) as to maintain near-to-adiabatic conditions. A silicone stopper with three openings was used: two main openings served as air inlet and outlet, while a smaller opening allowed for real-time temperature measurement via a sensor. To ensure airflow direction from bottom to top, a tube was inserted into the centre of the vessel, extending to its lowest part for optimal air distribution. During the experiments, the oxygen content in the exhaust air was monitored, and the OUR was calculated. Additionally, temperature evolution inside the Dewar was tracked using button sensors.

The accumulated heat (W) in the calorimeter was calculated using the equation proposed by Cooney et al., (Cooney et al., 1968):

$$Q_{acc}=K\cdot S \quad (2)$$

where K is the heat capacity of the system (J °C^{-1}) and S the heating rate (°C s^{-1}). The system's heat capacity was determined by summing the heat capacities of the solid and the calorimeter. The heating rate was obtained from the slope of the temperature-time curve, based on the observed temperature increase due to metabolic heat production. Once metabolic activity decreased, the heating rate declined accordingly. Finally, the metabolic heat yield (J g^{-1} O_2) was calculated from the slope of the accumulated heat versus the oxygen consumption rate. A preliminary test was conducted to assess the adiabatic performance of the calorimeter. For this, 450 mL of ultrapure water at 50 °C was added to the vessel, which was sealed with the silicone stopper, and the temperature evolution was monitored over time. To account for heat losses, a heat loss term (Q_L) was introduced into the energy balance of the solid phase (Supplementary material S4). This term was estimated using the experimental temperature profile and the *fminsearch* optimization tool in Matlab. The resulting heat loss term reflects the thermal losses associated with the calorimeter's silicone cap and aeration ports and was subsequently incorporated into the final energy balance. The heat loss transfer coefficient was estimated as 13.68 ± 0.23 W m^{-3} °C^{-1}. Thes equipment was used for the estimation of metabolic heat and mass and energy transfer coefficients as described below.

2.7. Mass and energy coefficients

The methodology described by Finkler et al., (Finkler et al., 2021) was adapted and implemented in our system for the experimental estimation of heat and mass transfer coefficients using the experimental temperature profiles at the central point of the calorimeter. Equations are described in Supplementary Material, S5-S8. A total set of six cooling experiments were performed by placing 68 g of solids at 40–54 °C in the calorimeter, supplying cool air (room temperature) and monitoring temperature evolution. Two significant modifications were introduced to the original methodology. First, the cooling experiment was conducted under near-to-adiabatic conditions in a 0.5 L calorimeter, instead of a non-isolated bioreactor, to prevent heat dissipation to the surroundings. Second, the solid sample was inoculated to maintain the same nutrient composition and moisture content as in the fermentation process. The inoculated mixture was prepared as described in Section 2.3 and then autoclaved at 121 °C for 20 min for these abiotic experiments. The calorimeter was supplied with humidified air at 30 mL min^{-1}, and the system's temperature evolution was recorded using button sensors (Thermochron iButton, Maxim Integrated, U.S.).

2.8. Kinetic model and yields estimation

2.8.1. Biomass estimation

Biomass was measured using the ergosterol content and the total colony-forming units (CFUs). Before ergosterol extraction, all samples were ground to minimize variability. Each sample was analysed in duplicate for a more accurate ergosterol quantification, following the methodology described by Rodríguez et al., (Rodríguez-Rodríguez et al., 2010). For extraction, 0.5 g of each sample was placed in a 15 mL glass centrifuge tube (KIMBLE HS), and 1 mL of cyclohexane along with 3 mL of a 10% w v^{-1} KOH solution in methanol were added. The extraction process consisted of two steps: first, samples were sonicated in an ultrasonic bath (P Selecta Ultrasons) for 15 min, followed by incubation in a thermostatic bath (Osaka TS) at 70 °C for 90 min. Afterward, 1 mL of distilled water and 2 mL of cyclohexane were added, and the tube was vortexed for 30 s at 35 Hz, then centrifuged at 3500 rpm for 5 min at 16 °C. The organic phase was transferred to a new 5 mL vial using a glass Pasteur pipette. This extraction step was repeated twice more by adding 2 mL of cyclohexane to the aqueous phase. The collected organic phase was stripped with nitrogen at 60 °C using a dry block heater. The residue was then dissolved in 1 mL of methanol at 40 °C for 15 min, vortexed for 30 s at 35 Hz, and transferred to 1.5 mL Eppendorf tubes. The samples were subsequently centrifuged (Fisher Scientific AccuSpin Micro) at 6000 rpm for 3 min at 4 °C, and the supernatant was transferred to amber HPLC vials. Ergosterol analysis was performed using a Dionex 3000 Ultimate HPLC equipped with a UV detector at 282 nm. Each sample (40 µL) was injected into a Kinetex 5 µm EVO C18 100 Å column (250 mm × 4.6 mm). The mobile phase was acetonitrile, and Chromeleon software was used for data analysis.

Total dry biomass and total CFUs were measured at different inoculum concentrations of *S. bombicola* (200, 400, 600, 800, and 1000 µL). For higher concentrations, the inoculum was centrifuged and diluted with liquid medium at 50% and 10%. A calibration curve was generated to correlate total dry biomass with total CFUs by extracting from a solid inoculated with a known amount of dry biomass. For dry biomass determination, different inoculum concentrations were placed in 1.5 mL Eppendorf tubes, centrifuged at 6000 rpm for 10 min at 20 °C, and the supernatant was discarded. The pellet was resuspended in 1 mL of water and transferred to pre-weighed aluminium trays, which were dried at 105 °C for 24 h before weighing. For CFU quantification, the same inoculum concentrations were added to pre-autoclaved solid substrate. Biomass extraction (1:10, w v^{-1}) was performed using Ringer solution (a sterile saline solution). The mixture was shaken in an orbital incubator at 200 rpm, 25 °C for 20 min and then serially diluted (1:10, v v^{-1}). Subsequently, 100 µL of each dilution was plated on agar and incubated at 30 °C for 48 h. After incubation, colonies were counted using a Schuette counter (Göttingen, Germany).

2.8.2. Kinetic model

The kinetic study was conducted by analysing CFU content at two-hour intervals during the microorganism's exponential growth phase in 6 solid-state fermentations under controlled temperature and moisture conditions. The mass composition of the solid and the operational conditions were the same as described in Section 2.3. The initial biomass concentration in all experiments was 4.91 ± 2.36 × 10^9 total CFUs. The selected temperatures were 20, 25, 30, 35, and 38 °C, while the moisture content values were 0.635, 0.923 and 1.095 kg water kg^{-1} total dry solids.

Five packed-bed bioreactors were set up, and oxygen consumption was continuously monitored. Once the exponential phase began, a small solid sample (representing less than 10% of the total solid volume) was taken from one of the reactors for the analysis of both CFUs and

ergosterol content. The reactor was then reconnected to the oxygen supply. After two hours, a second solid sample was taken from the same reactor for the same analyses. Since sampling twice exceeded 10% of the total solid content, that reactor was no longer used for further sampling. This sampling strategy was then sequentially repeated with the remaining reactors, allowing for the analysis of two time-separated samples per reactor. This kinetic study also provided insights into the relationship between OUR and biomass production.

2.8.3. Elemental analysis

Elemental analysis of carbon, hydrogen, nitrogen and sulfur (C,H,N and S) in *S. bombicola* was conducted by combusting dried and ground samples at 1200 ºC in an oxygen atmosphere, followed by quantification through gas chromatography. The analysis was performed using a CHNS Thermo Scientific Flash 2000 analyzer at the *Servei d'Anàlisi Química* of UAB.

2.8.4. Metabolic heat yield

To calculate the metabolic heat yield, we followed the methodology developed by Cooney et al., (Cooney et al., 1968). In summary, this approach involves periodically measuring the rate of heat production and oxygen consumption throughout the fermentation process using a dynamic calorimetric technique. The heat capacity in the calorimeter (J h^{-1}) is determined from the system's heat capacity (J $°C^{-1}$) and the heating rate ($°C\ h^{-1}$) using temperature sensors. Then, by plotting heat accumulation against oxygen consumption, the resulting slope represents the metabolic heat yield (J mol^{-1} O_2). To apply this methodology, SSF was carried out in four parallel replicates in 0.5 L packed-bed bioreactors. Every 12 h, one reactor was sacrificed to gather samples at different metabolic activity points, then introduced into the calorimeter to monitor the temperature evolution and OUR.

2.8.5. Heat yield from growth and maintenance

Another important parameter of the energy balance is the metabolic heat generated due to the growth of the microorganisms (J kg^{-1} biomass). This parameter can be calculated either theoretically or experimentally. The theoretical approach of this parameter is based on the methodology described by J.E. Bailey and D.F. Ollis (James and Bailey.). This approach involves calculating the metabolic heat yield from oxygen consumption and the stoichiometry between oxygen consumption and the microorganism's cellular composition. Alternatively, this yield can also be calculated experimentally, based on the measurement of OUR and microbial growth.

Additionally, a term representing the heat generation from cellular maintenance was incorporated into the energy balance of the solid phase. This heat generation persists even if biomass concentration remains constant. Conventional models assume heat production depends only on biomass concentration changes, leading to incorrect predictions. For this reason, an additional term was added to the energy balance, as detailed in the supplementary material (equation S8). This term was calculated using Eq. (3), which relates the previously determined heat yield from oxygen consumption (R_b), and the specific basal oxygen consumption rate (m_o). It is also influenced by the total solid and biomass concentrations. The (m_o) term was estimated based on biomass and OUR data from time-course experiments conducted between 72 and 120 h, corresponding to the stationary growth phase.

$$Q_R\left(\frac{kW}{m^3}\right) = R_b\left(\frac{kJ}{kg\ oxygen}\right) \times m_o\left(\frac{kg\ oxygen}{kg\ biomass\ x\ time}\right) \times b\left(\frac{kg\ biomass}{kg\ dry\ solid}\right) \times S\left(\frac{kg\ dry\ solid}{m^3}\right) \quad (3)$$

2.9. Analytical methods

pH and dry matter (DM) were determined following standard methodologies. Glucose quantification was performed using a YSI 2950D biochemistry analyzer (YSI Inc./Xylem Inc., United States). For glucose analysis, samples underwent solid-liquid extraction (1:10 w v^{-1}) at 50 °C and 200 rpm for 15 min, followed by filtration through a 0.45 µm RC membrane filter. Fat content was analyzed using the standard Soxhlet extraction method, as described by the U.S. Environmental Protection Agency (Method 9071B). Before extraction, dried and crushed samples (5 g) were loaded into cellulose cartridges and extracted in a Soxhlet-E816 apparatus (Büchi Ibérica S.L.U, Spain) using sequential n-hexane extractions for 5 h. All analyses were conducted in triplicate. Porosity was estimated according to literature (Ruggieri et al., 2009). The full characterization of the initial solid mixture for fermentation is depicted in supplementary material Table S1.

2.10. Mathematical model validation and numerical solution

The adapted model by (Finkler et al., 2021) used for the estimation of heat and mass transfer coefficients, the adapted model by Casciatori et al., (Casciatori et al., 2016) used for the validation of the obtained parameters, and the sensitivity analysis are presented in Section 3.7.

The four partial differential equations of the mathematical model implemented by (Finkler et al., 2021) were solved using numerical differentiation with the *ode15s* solver in Matlab® R2022 (MathWorks Inc., Natick, Massachusetts, United States). Additionally, the *fminsearch* function in Matlab® R2022 was employed to estimate the transfer coefficients and the specific growth rate. On the other hand, to solve the four partial differential equations of the mathematical model implemented by Casciatori et al., (Casciatori et al., 2016), a set of ordinary differential equations were numerically integrated using the *ode15s* function in Matlab® R2022, applying the finite volume approximation.

3. Results and discussion

3.1. Thermal properties of the solids

Solid-state fermentation induces dynamic changes in the solid matrix due to microbial growth and airflow. Microbial activity leads to substrate consumption, generating concentration gradients and metabolic heat within the reactor. Additionally, airflow contributes to moisture loss in the solid (Jin et al., 2017). These factors suggest that the thermal properties of the solid, such as heat capacity and thermal conductivity, may change during fermentation due to variations in temperature and humidity. To assess these potential changes, both unfermented and fermented samples (after four days) were analysed to determine any significant differences. Besides, the effects of moisture content and compaction on thermal conductivity were examined.

3.1.1. Specific heat capacity

Fig. 1 shows that the peak value of specific heat capacity of the unfermented sample is 1.88 J g^{-1} $°C^{-1}$ at approximately 58 °C. In contrast, for the fermented sample, the peak shifts to 65 °C with a slightly lower value of 1.83 J g^{-1} $°C^{-1}$. However, within the mesophilic temperature range (25–45 °C), the specific heat capacity varies between 1.55 and 1.65 J g^{-1} $°C^{-1}$. This difference is below 10% and it is likely negligible. A sensitivity analysis of the model should confirm the potential effects of this variation. These values are comparable to those for wheat straw (Koh et al., 2023), for lignocellulosic support materials (1.3–2.4 J g^{-1} $°C^{-1}$) (Tansel, 2023) and for wheat (2.7–3.3 J g^{-1} $°C^{-1}$) (Vauris et al., 2022).

3.1.2. Thermal conductivity

Table 1 shows that the difference in thermal conductivity between the initial and fermented solid samples is negligible. However, a significant difference was observed when comparing the dry, compacted solid with the sample at the initial moisture (41.20%) and porosity conditions of the fermentation process. This confirms changes in solids composition such as fat reduction and biomass and SL increase are not

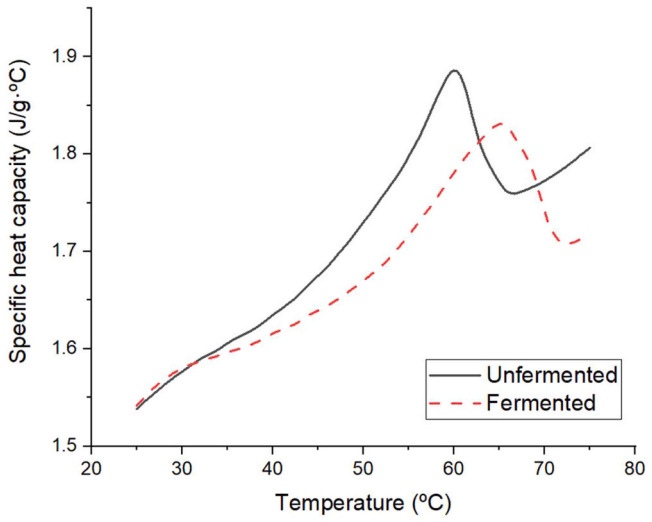

Fig. 1. Specific heat capacity of the samples at different temperatures.

Table 1
Thermal conductivity values for initial and fermented solids (average ± standard deviation).

Sample	Thermal conductivity (W m^{-1} °C^{-1})
Initial mixture (dry and compact)	0.0513 ± 0.0002
Fermented solid (dry and compact)	0.0515 ± 0.0001
Initial (wet and non- compacted)	0.1274 ± 0.0019

relevant, but a significant effect can be expected due to moisture gradients.

Reported values for agro-industrial SSF samples also show that thermal conductivity varies with moisture content. For example, sugarcane exhibits a thermal conductivity range of 0.057–0.439 W m^{-1} °C^{-1} at 7–80% moisture. Values for orange pulp and peel range from 0.158 to 0.269 W m^{-1} °C^{-1} at 6–75% moisture, while wheat bran falls within 0.210–0.326 W m^{-1} °C^{-1} at 3–37% moisture (Casciatori et al., 2013). Additionally, the thermal conductivity of wheat bran varies between 0.108 and 0.747 W m^{-1} °C^{-1} depending on its porosity, which ranges from 0.727 to 0.321 (Khanahmadi et al., 2005). This indicates that a higher free-air porosity results in lower bulk density and, consequently, reduced thermal conductivity, thereby playing a key role in heat dissipation (Teresa et al., 2024). However, due to differences in sample moisture content (dried vs. wet), the reported values are not directly comparable, making it difficult to isolate the effect of porosity alone. It is worth noting that the thermal conductivity values obtained in this study fall within the lower end of the ranges reported for other substrates, which may be related to the high fat content of the solids used in our system. Vegetable oils such as sunflower oil have thermal conductivities in the range of 0.17–0.21 W m^{-1} °C^{-1}, significantly lower than those of water-rich or fibrous materials.

3.2. Estimation of mass and energy transfer coefficients

Each fermentation has unique thermal properties of the solid matrix, involves different microorganisms and starts under varying initial conditions such as temperature or moisture content. These variations can affect the contact area at the solid-air interface, hindering the use of reported transfer coefficients (Mitchell et al., 2023). Thus, the methodology of (Finkler et al., 2021) was adapted to estimate the mass and heat transfer coefficients by fitting a heat and mass transfer model to data from cooling experiments under abiotic conditions. The model was modified to include a heat loss term in the energy balance equation to account for non-adiabatic conditions due to the calorimeter's silicone cap and aeration ports (equation S4). Fig. 2 shows the experimental and modelled solid temperature profiles during the cooling experiment. The heat transfer coefficient was $9.79 \times 10^3 \pm 2.25 \times 10^3$ W m^{-3} °C^{-1}, and the mass transfer coefficient was 0.00189 ± 0.00078 s^{-1} and they can describe the temperature decay under abiotic conditions.

These values are similar to, but lower than, those reported by (Finkler et al., 2021) for a mixture of wheat bran, sugarcane bagasse, and a solution of water with $(NH_4)_2SO_4$ which yielded an energy transfer coefficient of 1.68×10^4 W m^{-3} °C^{-1} and a mass transfer coefficient of 0.000211 s^{-1}. This difference could be attributed to the higher porosity of the mixture used herein (0.88 vs 0.56 m^3 m^{-3}), which results in a lower transfer area available per unit volume. In contrast, Von Meien and Mitchell (Von Meien and Mitchell, 2002) reported a heat transfer coefficient of 4.73×10^3 W m^{-3} °C^{-1} by using empirical equations derived from maize grain drying processes. This lower value is likely related not only to the higher particle size and density of corn grain, but also to differences in bed structure and flow conditions between grain drying and SSF systems.

3.3. Biomass estimation

Ergosterol and total CFUs were selected for biomass quantification. Other established methods, such as protein content analysis were discarded because it could lead to overestimated results, as yeast extract is present in the fermentation medium. Consequently, the measured protein would reflect not only the microbial protein but also the protein from the yeast extract (Abdul Manan and Webb, 2018). Ergosterol is an important sterol component of cell and mitochondrial membranes and has been used to estimate fungal biomass concentration in various biological processes (Nout et al., 1987; Rodríguez-Rodríguez et al., 2010; Mille-Lindblom et al., 2004). This compound is also employed for quantifying yeast biomass and was selected in this study because the *Candida* species possesses the gene *ERG3* involved in ergosterol biosynthesis (Hirayama et al., 2020; Vella et al., 2023). Fig. 3 shows the correlation between dry biomass and both ergosterol concentration and CFUs, based on inoculum samples of different concentration.

The primary objective of determining the amount of biomass was to calculate the specific growth rate (μ). During the kinetic experiment, both ergosterol content and total CFU of all samples were collected during the exponential phase. However, the biomass estimates based on CFUs were consistently higher than those based on ergosterol. Several factors may explain the lower biomass estimates from ergosterol. Firstly, the physiological condition of yeast differs significantly between SSF

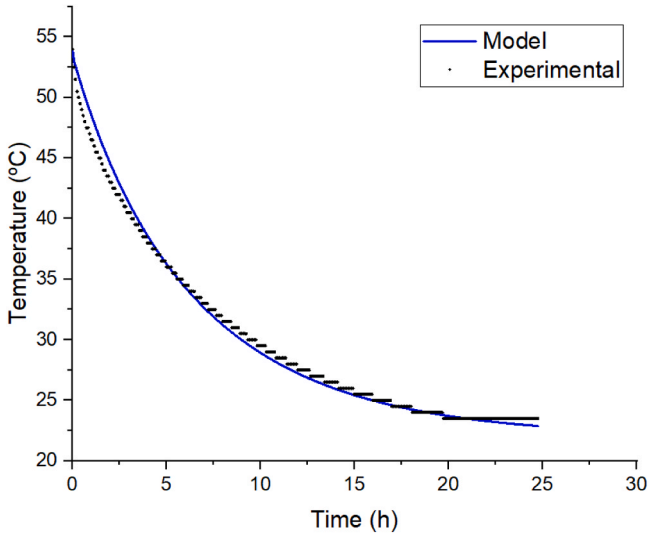

Fig. 2. Experimental and modelled temperature of the solid for transfer coefficient estimation.

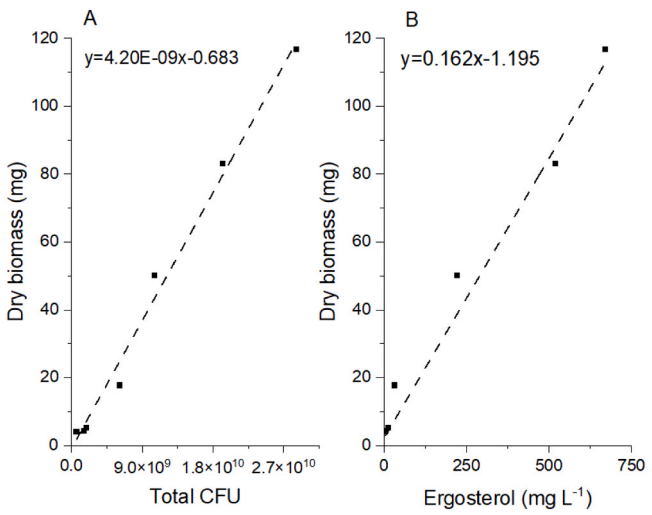

Fig. 3. Calibration curve of dry biomass versus (A) Total CFUs; (B) Ergosterol (mg L^{-1}).

and submerged fermentation (SmF) systems. In SSF, cells experience lower water activity, restricted oxygen diffusion, and heterogeneous nutrient distribution, which can affect membrane composition and reduce ergosterol synthesis. Secondly, SSF cells are more susceptible to environmental stress or may enter stationary or sporulation phases earlier, further lowering the ergosterol content per unit of biomass. Furthermore, the solid matrix in SSF might impede solvent diffusion and reduce extraction efficiency, leading to an underestimation of total ergosterol. These combined effects suggest that the ergosterol-to-biomass ratio is not consistent across fermentation methods and requires specific calibration for each system. Although ergosterol is widely used for biomass estimation in filamentous fungi, its application to yeast remains poorly explored. In a previous study analysing biomass content by ergosterol measurement in six fungal species and three yeast strains, it was observed that ergosterol measurement tends to underestimate biomass in yeast (Pasanen et al., 1999). The lower ergosterol content per yeast cell is likely due to the higher cell concentration per dry mass in yeast cultures compared to spore concentrations in filamentous fungi. These findings support the view that ergosterol is a reliable indicator of biomass for filamentous fungi, but less appropriate for yeast species.

For this reason, CFUs analysis was selected for this study, due to the robustness of this parameter when quantifying the viable cell numbers of the specific microorganism. Moreover, it allows detection of potential contamination during fermentation.

3.4. Kinetic model

3.4.1. Growth rate

Currently, no specific growth rate values are available in the literature for *S. bombicola* in SSF systems. Although data exist for SmF, these values are highly dependent on fermentation conditions such as substrate type and stirring speed, and therefore cannot be reliably applied to solid-state systems. The variability of growth rates across fermentation types and conditions underscores the need for precise, system-specific growth measurements. Determining the growth rate under SSF conditions thus enhances the robustness and reliability of the modelling approach.

Maddikeri et al., (Maddikeri et al., 2015) analysed the effect of using waste cooking oil as a sustainable carbon source in a SmF under varying stirring speeds on microbial growth and SL production under various fermentation conditions. Increasing the stirring speed from 150 rpm to 300 rpm resulted in a rise in the specific growth rate from 0.053 h^{-1} to 0.058 h^{-1}, attributed to reduced gas-liquid mass transfer resistance and enhanced transport of biomass and carbon sources. However, any further increase in stirring speed did not lead to additional improvements, possibly due to the fact that the mass transfer is no longer the rate controlling mechanism above 300 rpm (Maddikeri et al., 2015). The use of a pure substrate, such as sunflower oil, was also analysed. In this case, the specific growth rate was 0.14 h^{-1}, representing a 59% increase compared to fermentation with waste oil. Yeast extract concentration also influenced growth, with low concentrations leading to minimal biomass accumulation and specific growth rate ranging from 0.14 h^{-1} to 0.15 h^{-1}(García-Ochoa and Casas, 1999). These studies highlight the sensitivity of μ to process variables and reinforce the need to experimentally determine growth kinetics for each system.

The logistic Eq. (4) is commonly used in SSF works (Mitchell et al., 2004) and it was selected to describe the yeast growth rate in Fig. 4.

$$\frac{dX}{dt} = \mu \cdot X\left(1 - \frac{X}{X_{max}}\right) \quad (4)$$

The specific growth rate was calculated from biomass measurements taken during the exponential phase of fermentation. Fig. 4 shows both biomass accumulation and COC during the lag phase. As the figure shows biomass levels remain stable during the first 10 h, corresponding to the lag phase, when cells are adapting to the medium and operating conditions. Around hour 10, the exponential phase begins and continues until approximately hour 24, when the stationary phase is reached. COC profiles match those of biomass. All kinetic experiments were concluded at this point, as biomass data from the stationary phase are not suitable for calculating μ.

Based on the data presented in Fig. 4, the specific growth rate was calculated as 0.389 h^{-1}. This value is substantially higher than the values for SmF described reported, which is consistent with other studies comparing submerged and solid-state systems. For example, in a comparative study on *Aspergillus niger,* SmF growth rates ranged from 0.083 h^{-1} to 0.091 h^{-1}, whereas SSF values were significantly higher, ranging from 0.236 h^{-1} to 0.323 h^{-1}, an increase from 62% to 75%. These differences are attributed to variations in water content and dissolved oxygen, which influence interactions between biomass and the culture medium (Favela-Torres et al., 1998). A separate study further demonstrated that both temperature and initial moisture content influence growth kinetics in SSF. At higher moisture levels, reduced porosity can limit oxygen diffusion, negatively affecting growth. As expected, the specific growth rate was found to depend strongly on both variables (Hamidi-Esfahani et al., 2004).

3.4.2. Growth dependence on temperature

Preliminary experiments showed that at 42 °C, the OUR dropped

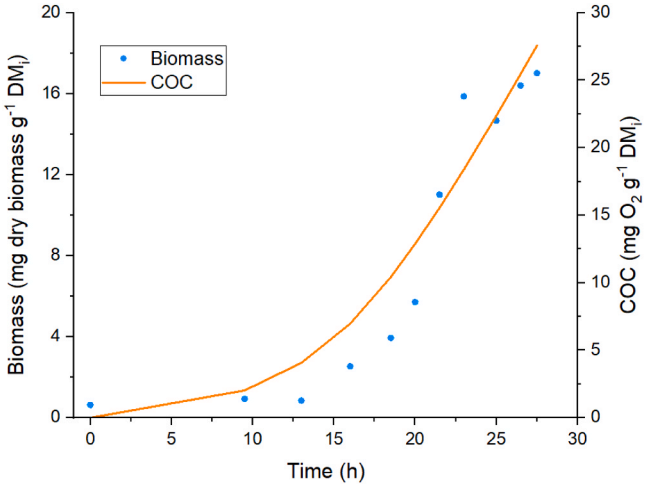

Fig. 4. Biomass and COC profile of the kinetic experiment at the optimal conditions.

sharply because *S. bombicola* could not withstand such high temperatures. The profile of the temperature is presented in the supplementary material (Figure S2). Therefore, 38 ºC was chosen as the upper limit. Fig. 5A shows the OUR profiles at different temperatures. The profiles at 25 ºC and 30 ºC are practically identical, indicating that *S. bombicola,* a mesophilic strain, has an optimal temperature range between these temperatures (Vedaraman and Venkatesh, 2010). However, growth at 30 ºC showed slightly better adaptation, aligning with other studies on SL production via SSF, which typically use this temperature as a standard operating condition (Rodríguez et al., 2021; Jiménez-Peñalver et al., 2016). At 35 ºC, OUR decreased, suggesting that microbial growth is reduced at high temperatures. This effect was even more pronounced at 38 ºC, where OUR dropped by 64% compared to 30 ºC, confirming the strain's thermal sensitivity. On the other hand, at 20 ºC, an extended lag phase was observed, during which OUR remained low. Although cells eventually adapted, the overall metabolic activity remained limited. The lowest OUR values were recorded at the temperature extremes (20 ºC and 38 ºC), accompanied by significantly reduced CFU counts—up to one order of magnitude lower than at optimal temperatures.

The values from the exponential phase were used to calculate the specific growth rate at each temperature (Fig. 5B). Eq. 5, a commonly applied correlation to model microbial growth in SSF systems (Hamidi-Esfahani et al., 2004) was fitted to the experimental data yielding the following parameters: $A = 4.11 \times 10^{7}\ s^{-1}$, $B = 8.78 \times 10^{46}$, $E_{A1} = 68577\ J\ mol^{-1}$, $E_{A2} = 27444\ J\ mol^{-1}$.

$$\mu_T = \frac{1}{\mu_{opt}} \frac{A \times \exp\left(\frac{-E_{A1}}{R[T+273]}\right)}{1 + B \times \exp\left(\frac{-E_{A2}}{R[T+273]}\right)} \quad (5)$$

At 35 ºC, μ decreased by 33% compared to the 30 ºC and at 38 ºC, it dropped to a level comparable to that observed at 20 ºC. These results suggest that growth outside the 20–38 ºC range is negligible, supporting the suitability of the selected range for kinetic modelling.

3.4.3. Growth dependence on water content

Moisture is another key parameter influencing the specific growth rate, as observed in previous studies. In this work, OUR, total CFUs, and specific growth rate were analysed at the reference moisture level (75% of water holding capacity, equivalent to 0.923 g water g^{-1} dry solids) (Rodríguez et al., 2021), as well as at two additional levels: 50% (0.635 g water g^{-1} dry solids) and 90% WHC (1.095 g water g^{-1} dry solids). Fig. 6 shows the OUR profiles obtained for these three conditions. The OUR at the reference value reached a higher peak, and the exponential phase is shorter compared to the other conditions. At 50%, a longer lag phase was observed, indicating that the low moisture content

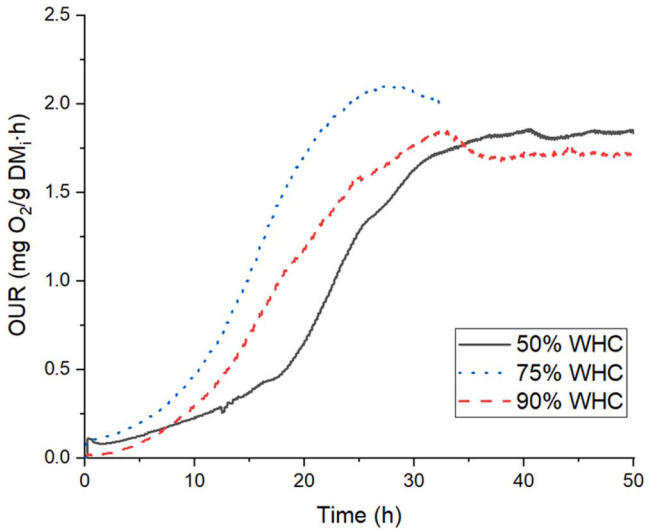

Fig. 6. OUR profile at different values of water holding capacity.

delayed microbial adaptation. Nevertheless, OUR values at 50% were higher than those observed at 90%. At 90%, the lag phase was similar to the reference value, but the OUR values obtained were lower.

The effect of moisture content on the specific growth rate was quantified using Eq. 6, resulting in a coefficient of determination (R^2) of 0.987:

$$\mu_W = 0.73W_s - 0.264 \quad (6)$$

At 50% WHC, the specific growth rate was a 46.9% lower than the reference value observed at 75% WHC. In contrast, increasing the moisture content to 90% led to a 29.1% increase compared to the reference. At 50%, the specific growth rate reached values similar to those obtained at 20 and 38 ºC. This indicates that the moisture content of the solid is a critical parameter during fermentation, when the solid loses moisture by convection affecting the growth of the microorganism.

3.5. Yields

3.5.1. Heat yield from growth

Another key parameter is the yield relating metabolic heat production to oxygen consumption. This value, closely linked to microbial growth, was experimentally determined under specific conditions for fermentation. Monitoring the OUR is essential, as it reflects both microbial activity and heat generation potential. Calorimetric experiments

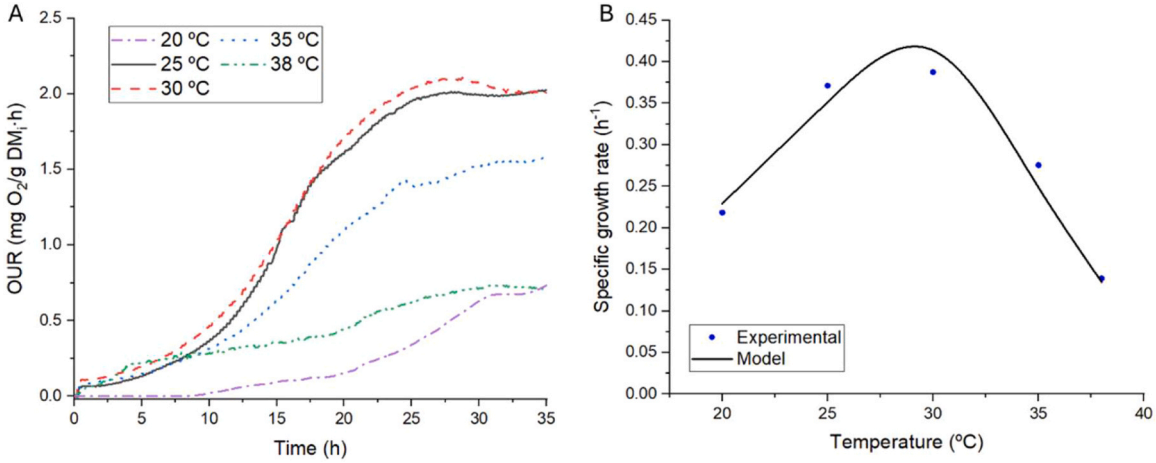

Fig. 5. A) OUR at different temperatures; B) Experimental and simulated specific growth rate at different temperatures.

conducted in this study yielded a value of 9400 J g^{-1} O_2 ± 263 J g^{-1} O_2. Literature reports a value of 16250 J g^{-1} O_2 for *Aspergillus niger*(Finkler et al., 2021) and a value of 14375 J g^{-1} O_2 (Cooney et al., 1968). Although few reference values are available, the value obtained in this work falls within a reasonable range relative to previously reported data. These results highlight the importance of experimentally determining system-specific values.

This heat yield from growth must be expressed in biomass mass units rather than in terms of oxygen consumed. This conversion can be achieved through both experimental and theorical approaches. One of the methods involves using a coefficient that relates biomass to oxygen consumption: 1.314 kg of oxygen consumed per kg of biomass was obtained by the kinetic study showed in Fig. 4. Then, the calculated heat yield from growth is 1.24 × 10^7 J kg^{-1} biomass.

On the other hand, the heat yield from growth can be calculated using the methodology developed by James E. Bailey and David F. Ollis (James and Bailey). For this approach, the elemental composition of *S. bombicola*, determined through C, H, N, S elemental analysis, was used to rewrite its empirical formula. The cellular composition was quantified in molar percentages, and these values served as the basis for recalculating the remaining stoichiometric coefficients in the overall reaction equation. The following equation was the result of this analysis.

$$CH_{1.79}N_{0.14}O_{0.62} + 1.14O_2 \rightarrow CO_2 + 0.07N_2 + 0.9H_2O \quad (7)$$

Eq. 8 represents the estimation of the metabolic heat produced per unit of biomass based on the overall stoichiometry of biomass oxidation in Eq. 7. The calculation uses the stoichiometric coefficients for biomass and oxygen consumption, together with the metabolic energy released per mole of oxygen consumed (3.01 ×10^5 J mol^{-1} O_2), which corresponds to the value of 9400 J g^{-1} O_2, as determined from the calorimetric experiments described above. The total biomass mass is estimated from the elemental composition of the biomass (C, H, N, O). Thus, the heat produced per kilogram of biomass is obtained as:

$$\frac{(1.14\text{mol}O_2)(3.01\text{x}10^5 \frac{\text{J}}{\text{mol}O_2})}{[12 + (1.79)(1) + (0.14)(14) + (0.62)(16)]\text{g}} = 1.34\text{x}10^7 \frac{\text{J}}{\text{kg biomass}} \quad (8)$$

This approach allows converting the heat released per mole of oxygen consumed into a specific heat production coefficient (J kg^{-1} biomass), which is then used in the energy balance for the SSF system.

Both yields values obtained are very similar and fall within the range of values reported in the literature (Finkler et al., 2021; Casciatori et al., 2016; Von Meien and Mitchell, 2002). A sensitivity analysis performed in the Section 3.7 will help to choose the suitable value. Although only two specific yield values are commonly cited, they are frequently applied across SSF modelling studies regardless of the microorganism involved. For instance, a yield of 8.36 × 10^6 J kg^{-1} biomass determined for *Rhizopus oligosporus* (Sargantanis et al., 1993) was also used in a modelling study involving the thermophilic fungus *Myceliophthora thermophila* (Casciatori et al., 2016). Similarly, a yield of 1.54 × 10^7 J kg^{-1} biomass from *Gibberella fujikuroi (*Mitchell, 2006*)* was adopted in a model simulating *Aspergillus niger* (Finkler et al., 2021). Based on the stoichiometric equation for the growth of *S. bombicola,* the yield of water produced per unit of biomass can be calculated. The resulting yield is 0.63 kg water kg^{-1} biomass.

3.5.2. Basal metabolic heat

The term corresponding to metabolic heat production of the solid phase in the energy balance was modified because it commonly assumes that heat production depends mainly on the heat produced linked to biomass growth (Casciatori et al., 2016; Von Meien and Mitchell, 2002). However, this formulation implies that if there are no changes over time in biomass concentration, the metabolic heat term becomes null. While this may be appropriate for modelling the exponential growth phase, it fails to capture metabolic heat production during the stationary phase. In the present study, where the target product is a secondary metabolite predominantly synthetized during the stationary phase, it was essential to incorporate this stationary stage into the model. To address this limitation, a basal heat production term was incorporated to represent ongoing cellular respiration and maintenance, which continue to produce heat even after the maximum biomass concentration has been reached. This modification is consistent with experimental data showing sustained metabolic heat production beyond the growth phase. The mathematical formulation of this maintenance-associated heat term is provided in the supplementary material (S8). This yield was determined based on the OUR and biomass profiles obtained during the time course experiment, specifically within the 72–96 h range. This period corresponds to the temperature range where the biomass derivative remains constant. The residual metabolic heat term was found to be 110 W kg^{-1} biomass.

3.5.3. Substrate/biomass and product/substrate yields

During the solid-state fermentation process, *S. bombicola* uses glucose as a hydrophilic carbon source for growth during the exponential phase. In contrast, SL production requires the metabolism of a hydrophobic carbon source, which in this study is the oil present in the winterization oil cake. Although the yeast can also grow on glycerol released from triglyceride hydrolysis, for simplification, it was assumed that growth occurs only on glucose, while fat is hydrolysed during the stationary phase, coinciding with SL production.

The glucose/biomass yield, $Y_{g/b}$, defined as the amount of glucose consumed per unit of biomass produced, was determined under reference conditions (30 ºC and 75% WHC), yielding 2.88 g glucose g^{-1} biomass (Supplementary material Figure S3). Substrate/biomass yield reports for *S. bombicola* in SSF are scarce in the literature. A value of 2.17 g glucose g^{-1} biomass has been reported for SmF using in a 1 L shake flasks (Ribeiro et al., 2013), which is 24% lower than the value obtained here. In SmF, the homogeneity of the liquid medium facilitates enhanced substrate availability and uptake. In contrast, the inherent heterogeneity of SSF results in the development of nutrient concentration gradients, limiting substrate availability and accessibility to the biomass. This difference in glucose distribution is a key factor explaining the disparity in yield between the two systems. Moreover, such gradients can cause localized metabolic variations, which remain a major challenge in SSF scale-up (Rahardjo et al., 2006).

Previous studies on SL production through SSF have highlighted the critical role of fat content in enhancing yield. In particular, one study reported that an optimal hydrophobic to hydrophilic substrate ratio of 1:4- corresponding to the highest fat and lowest sugar content – resulted in the highest SL production (Jiménez-Peñalver et al., 2016). Similarly, in a comparative analysis using various hydrophobic waste-derived substrates, the oil cake with the highest fat content led to the greatest SL yield, further reinforcing the importance of fat-rich substrates in optimizing SL biosynthesis under SSF conditions (Eras-Muñoz et al., 2024). In fact, SL biosynthesis begins with lipase activity, which promotes the liberation of fatty acids, as SL production is directly linked to fats degradation during the stationary phase of fermentation (Celligoi et al., 2020).

For this reason, in this study, two key yields were determined: the crude SL yield based on consumed fat. Notably, studies in the literature frequently report SL production yields related to the total amount of the substrates consumption, such as 0.175 g SL g^{-1} substrate (Parekh et al., 2012). However, specific data on crude SL yield relative to fat utilized in fermentation are limited. Under the evaluated fermentation conditions, a yield of 0.73 g crude SL g^{-1} fat was obtained (Supplementary material Figure S4). These results are consistent with a previous study using the same substrates, where a yield of 0.8085 g SL g^{-1} fat was reported (Jiménez-Peñalver et al., 2016). The composition of the oil—particularly fatty acid chain length and degree of unsaturation—has been shown to significantly influence SL production (Felse et al., 2007).

3.6. First simulations of the mathematical model

Once all system-specific parameters had been determined, they were validated by comparing the mathematical simulation with the experimental temperature data measured at three axial positions (z/L=0.18; z/L=0.55 and z/L=0.91) and three radial positions (r/R=0; r/R=0.5; r/R=1) of the reactor. The implemented mathematical model was based on the same mass and energy balances described by Casciatori et al., (Casciatori et al., 2016) considering the modifications specified in supplementary material (S8).

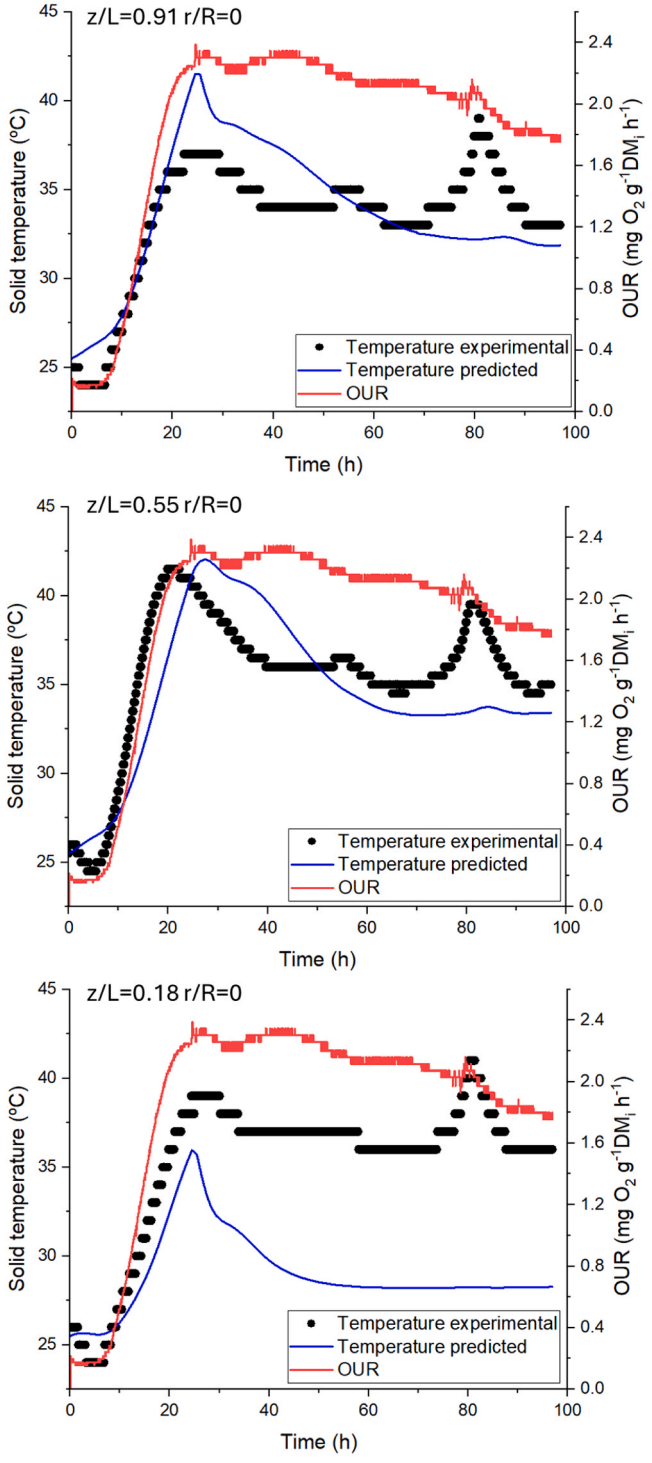

Fig. 7. Experimental and simulated profile of the solid temperature and OUR along the axial axis of the reactor.

At the bottom part of the reactor (z/L=0.18) (Fig. 7), both the temperature and oxygen consumption profiles exhibited exponential increases during the first 24 h of fermentation. The rise in oxygen consumption is correlated with glucose consumption, which promoted biomass accumulation within the reactor and raised the solid temperature due to the generated metabolic heat. A subsequent decrease of approximately 2 °C at around 24 h coincided with the increase in airflow rate, after which the temperature remained relatively stable, reflecting a balance between metabolic heat generation and heat dissipation. Two temperature peaks were observed, due to direct sunlight entering the laboratory. The simulated profile followed the same pattern, with an initial increase followed by a pronounced decrease after 24 h. However, the maximum simulated temperature was ~7 ºC lower than the experimental, and the model predicted a sustained decline of ~28 ºC, suggesting an overestimation of energy losses associated with water evaporation from the solid to the air. This aligns with previous studies predicting the lowest temperature in the bottom of the reactor (Rodrigues et al., 2022). As mentioned above, the effect of direct sunlight was also captured by the simulations, though the predicted peaks were smaller, likely because the room temperature sensor remained shaded and did not reflect the higher wall temperatures caused by solar exposure. This effect was observed across all three axial positions within the reactor.

Fig. 7 (z/L=0.55) presents the OUR, the experimental solid-phase temperature at the reactor centre, and the simulated temperature profile for the 22-L bioreactor. The temperature peaked at 42.5 ºC, exceeding the optimal growth range and the critical threshold of 38 ºC associated with cell death, as identified in the kinetic study. To mitigate this rise, airflow was increased at 24 h, resulting in a 6.5 ºC drop over 16 h. This decrease was attributed to enhanced convective heat transfer, which facilitated dissipation from the solid to the gas phase. Subsequently, the temperature stabilized at 35–36 °C until the end of the fermentation. This behaviour can be explained by several factors. First, both oxygen consumption and biomass accumulation entered a stationary phase around 60 h, indicating a stabilization of biomass production. Consequently, heat production became primarily associated with maintenance respiration, which generates less metabolic heat. These effects explain the ~6 ºC drop observed between 24 and 40 h. However, due to the low thermal conductivity of the solid substrate, residual heat could not be fully dissipated, and the temperature remained within this range until the end of the process.

Model validation against experimental data showed good agreement. Both experimental and predicted temperature profiles reached similar peak values, with the model estimating a maximum value 2 ºC lower than the experimental measurement, which is considered acceptable. The predicted peak occurred 5 h later than the experimental one, but this discrepancy is within an acceptable range. Overall, the modelling approach and the experimentally determined coefficients are considered adequately validated. Both experimental and simulated profiles followed a similar pattern in the upper section of the reactor (z/L=0.91). The model overestimated the peak temperature by approximately 3 °C without delays. The simulated response to increased airflow at 24 h was consistent with the experimental observations.

The mathematical model was also validated at three radial positions. Temperature sensors were placed at different radial locations along the same axial level (z/L=0.5) to compare experimental measurements with simulation results. Fig. 8 shows the experimental and predicted temperature in three radial positions: at the centre (r/R=0), at the middle of the radius (r/R=0.5) and in the internal wall of the reactor (r/R=1). The model demonstrated a strong agreement with the experimental data across all radial positions, successfully replicating all temperature peaks observed during fermentation. Notably, it accurately predicted the temperature at the reactor's internal wall. Radial profiles revealed the steepest gradients near the walls, with maximum values of 42 ºC at r/R= 0 and 39 ºC at r/R= 0.5, compared to 28 ºC at the wall, indicating that heat accumulates at the centre and dissipates outward.

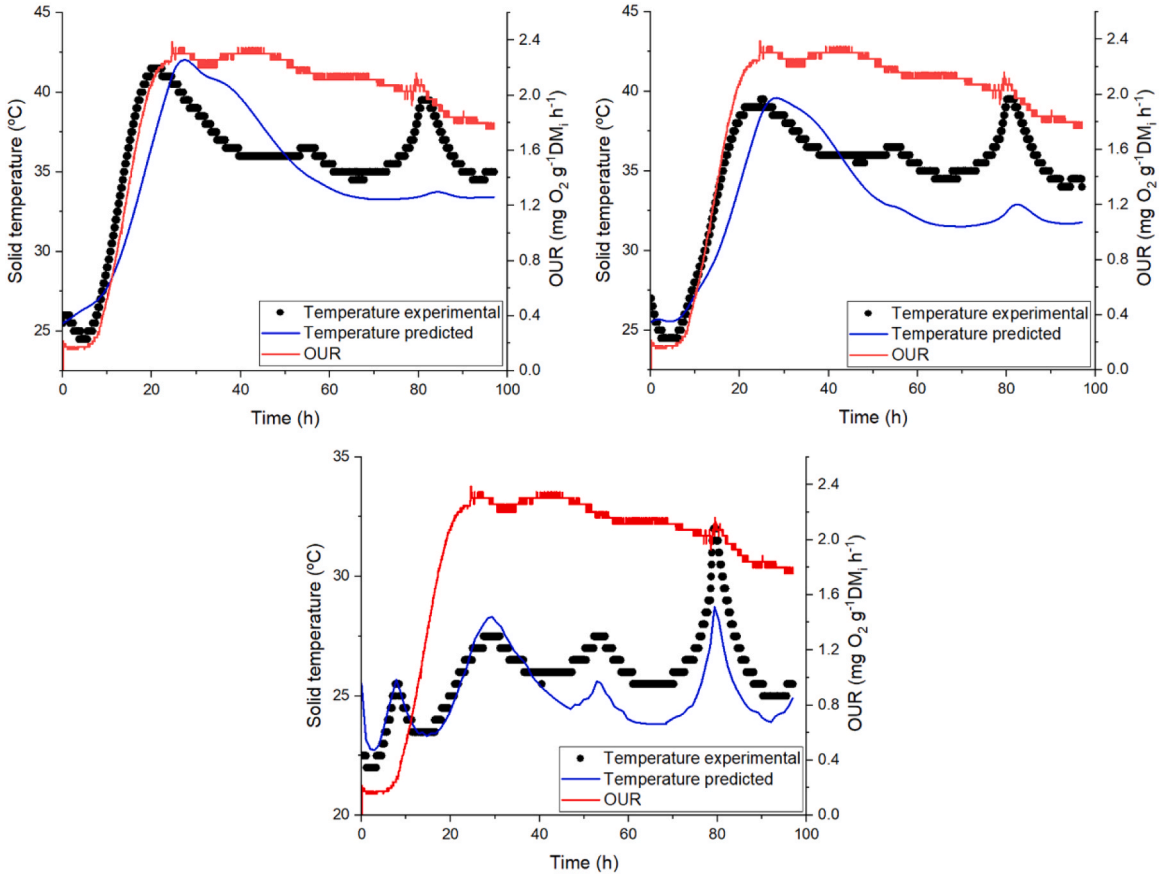

Fig. 8. Experimental and simulated profile of the solid temperature and OUR along the radial axis of the reactor.

To clarify the inclusion of the basal metabolic heat, Figure S5 (supplementary material) presents the experimental and simulated temperature profiles at the three axial positions, considering a basal metabolic heat equal to zero. At all three axial positions of the reactor, the simulated temperature increased, however, the peak temperature was lower than the experimental values. Furthermore, once this maximum temperature was reached, the simulated profile decreased abruptly until it approached the inlet air temperature. This temperature dynamic occurs because the metabolic heat term in the balance is directly related to the biomass growth. During the stationary phase, however, the biomass remains nearly constant, causing this term to become negligible. For this reason, the basal metabolic heat term during the stationary phase of microbial growth was incorporated into the energy balance of the solid phase.

Although the model accurately predicts the solid temperature profile, this is only a first step in the modelling process. To validate the reliability of the estimated parameters and assess the model's suitability for scale-up, a sensitivity analysis is required. This analysis helps identify how variations in specific parameters and operating conditions affect the model's predictions.

3.7. Sensitivity analysis

The mathematical model includes numerous parameters that influence the accuracy of its predictions. To evaluate the impact of each, a sensitivity analysis was performed using both experimentally determined and literature-based values. The Euclidean norm and absolute error between the experimental and simulated solid temperatures at the centre of the reactor were calculated. The parameters selected for analysis included the specific heat capacity, thermal conductivity, heat yield from growth, microbial kinetic parameters (specific growth rate, A, B, E_{A1}, E_{A2}), and the mass and heat transfer coefficients. Each parameter was varied by −50%, −25%, + 25%, and + 100% from its experimental

Table 2
Euclidean norm and absolute error of the sensitivity analysis. For reference values, Norm is 92.23 °C and error is 2.38%.

Parameter	Reference value	Norm (°C) and absolute error (%)			
		-50%	- 25%	+ 25%	+ 100%
Heat capacity (J g^{-1} °C^{-1})	1.55	88.30	90.58	95.11	101.25
		2.32	2.36	2.45	2.55
	1.65	88.72	91.16	96.05	101.30
		2.33	2.37	2.47	2.87
Thermal conductivity (W m^{-1} °C^{-1})	0.127	84.97	88.72	97.99	116.09
		2.23	2.31	2.51	2.87
Heat yield from growth (J kg^{-1} biomass)	1.24×10^7	144.72	112.86	93.20	138.99
		3.45	2.62	2.46	3.25
	1.34×10^7	137.87	106.49	97.32	152.75
		3.28	2.46	2.54	3.58
Specific growth rate (h^{-1})	0.39	274.42	257.34	235.76	233.43
		7.44	7.11	6.51	6.11
A (s^{-1})	4.11×10^7	154.77	113.68	86.50	113.14
		3.13	2.58	2.35	2.91
B	8.78×10^{46}	93.91	93.15	93.40	98.26
		2.52	2.46	2.34	2.30
E_{A1} (J mol^{-1})	68577	571.36	495.14	405.24	407.49
		8.65	8.51	11.15	11.21
E_{A2} (J mol^{-1})	27444	407.49	407.49	160.85	160.85
		11.21	11.21	3.40	3.40
Mass transfer coefficient (s^{-1})	0.0019	92.46	92.33	92.10	91.79
		2.39	2.38	2.37	2.36
Heat transfer coefficient (W m^{-1} °C^{-1})	9790	93.03	93.32	92.15	92.44
		2.41	2.36	2.37	2.39

value. Results are summarised in Tables 2 and 3. For this, we will focus on the temperature profile of the solid, which is a crucial variable for reactor scale-up.

The first parameter analysed was the specific heat capacity of the solid. As mentioned above, the experimental range was 1.55 and 1.65 J g^{-1} °C^{-1}. When no variation was applied to this parameter, the predicted norm temperature and absolute error were 92.23 ºC, and 2.38%, respectively, for a value of 1.55 J g^{-1} °C^{-1}; 93.00 ºC and 2.40%, respectively, for a value of 1.65 J g^{-1} °C^{-1}. As observed in Table 2, an increase in specific heat capacity led to higher norm and absolute error values, however, the maximum variability between these values was approximately 10%, indicating that this parameter is not sensitive within the model. Given the negligible difference, a value of 1.55 J g^{-1} ºC^{-1} was selected for further analyses. In this case, the reported bibliographic range for specific heat capacity (1.45–3.14 J g^{-1} ºC^{-1}) lies within the range observed in the tests (Vauris et al., 2022).

A similar pattern was observed for thermal conductivity, although with higher variation (up to 20%). Increasing thermal conductivity led to a simulated temperature profile that underestimated experimental data, due to enhanced heat dissipation. For example, using the literature value of 0.747 W m^{-1} °C^{-1} (porosity 0.321) resulted in a norm 59.87% higher than the one obtained with the experimental value (porosity of 0.88 m^3 voids m^{-3} bed). These results highlight the importance of selecting reference values aligned with the physical properties of the specific SSF system (e.g., porosity, moisture).

In contrast, modifying the heat yield from growth had a strong impact, with changes in the norm and error reaching up to 50% (Figure S6). Higher yields increased solid temperature due to greater metabolic heat generation, while lower yields produced the opposite effect. Literature values of 8.36 × 10^6 J kg^{-1} biomass and 1.54 × 10^7 J kg^{-1} biomass (Finkler et al., 2021) fall within the tested range. These results highlight the strong influence of this parameter on model accuracy and suggest that relying solely on literature values may lead to significant deviations from experimental data.

Similarly, the model proved highly sensitive to variations in the specific growth rate of *S. bombicola* under SSF conditions, with norm and error values increasing up to 2.5-fold (material supplementary Figure S7). Using the SmF-based value of 0.14 h^{-1} resulted in substantial norm and error increases (Table 3), reinforcing the need for system-specific experimental determination.

The equation that relates the specific growth rate to temperature involves four parameters (A, B, E_{A1} and E_{A2}). Varying A by + 25% slightly improved the norm, but a + 100% increase raised the norm by 22.7%, while a −50% decrease raised it by 67.8%. Using the bibliographic value of 2.69 × 10^7 s^{-1} resulted in a 6.19% error. In contrast, variations in B had negligible effects, suggesting that this parameter does not require precise experimental determination. On the other hand, the activation energy terms showed high sensitivity to the model, confirming their critical role in describing temperature dependence (Table 2). Small variations led to large deviations in the model output, indicating that both coefficients must be estimated experimentally.

Table 3
Euclidean norm and absolute error of bibliographic values.

Parameter	Value	Norm/ Error	Reference
Thermal conductivity (W m^{-1} ºC^{-1})	0.747	229.83/ 6.25	(Khanahmadi et al., 2005)
Specific growth rate (h^{-1})	0.14	290.47/ 7.77	(García-Ochoa and Casas, 1999)
A (s^{-1})	2.69 × 10^7	232.99/ 6.19	(Casciatori et al., 2016)
B	1.30 × 10^{47}	94.78/ 2.33	(Finkler et al., 2021; Casciatori et al., 2016; Von Meien and Mitchell, 2002)
E_{A1} (J mol^{-1})	70225	167.79/ 3.28	(Casciatori et al., 2016)
E_{A2} (J mol^{-1})	28336	122.89/ 2.95	(Casciatori et al., 2016)
Mass transfer coefficient (s^{-1})	0.00021	92.70/ 2.40	(Finkler et al., 2021)
Heat transfer coefficient (W m^{-1} ºC^{-1})	16842	92.54/ 2.39	(Finkler et al., 2021)

Mass and heat transfer coefficients showed minimal effect on the solid temperature profile. Their variation did not significantly change norm or error values, although minor effects were observed in other variables, such as moisture content. Similar outcomes were obtained when using the bibliographic values reported by Finkler et al., (Finkler et al., 2021).

As shown in the previous section, the addition of the basal metabolic heat term proved to be critical, as confirmed by sensitivity analysis. For instance, at the central point of the reactor, the calculated norm was 92.23 °C with an error of 2.38% when basal metabolic heat was considered, whereas omitting this term resulted in a norm of 299.52 °C and an error of 7.73%.

Despite the continued use of literature-derived reference values in recent SSF modelling studies, this sensitivity analysis helps clarify which parameters must be experimentally determined for each specific system, and which can potentially be taken from existing data – particularly in the case of temperature prediction at the centre of the reactor. As previously discussed, thermal properties such as specific heat capacity and thermal conductivity showed only minor effects on the Euclidean norm and absolute error compared to reference values (92.23 ºC and 2.38%). For example, varying the specific heat capacity within the bibliographic range resulted in changes of less than 10%, suggesting that this parameter does not significantly influence the temperature profile. Similar observations have been reported in previous studies, where changing the heat capacity from 1.0 to 4.0 J g^{-1} °C^{-1} had negligible effects on solid temperature (Sangsurasak and Mitchell, 1998). Likewise, using literature values for thermal conductivity—appropriately adjusted to porosity and moisture—did not lead to substantial deviations. In another study, varying thermal conductivity from 0.03 to 1 W m^{-1} °C^{-1} also showed minimal influence (Sangsurasak and Mitchell, 1998). In summary, thermal property coefficients do not appear to require precise experimental determination, and bibliographic values may be considered acceptable—provided they are adapted to the physical characteristics of the system. This may help reduce the number of required experimental analyses and associated costs. The same applies to the mass and energy transfer coefficients, which showed low sensitivity in the model.

However, when multiple bibliographic values are applied simultaneously, specifically, using the thermal and transfer parameters reported by (Casciatori et al., 2016) while maintaining our own microbial kinetic data, the cumulative effect becomes significant. Under these conditions, the norm increases to 175.98 ºC and the absolute error to 4.74%, approximately doubling the baseline values, despite the microbial parameters being kept constant. This illustrates that even relatively insensitive parameters can collectively introduce substantial deviations if not selected carefully.

Figure S8 (supplementary material) compares the simulated temperature profiles obtained using experimentally determined model parameters, bibliographic parameters, and the experimental temperature profile. The bibliographic parameters used were taken from Casciatori et al., (Casciatori et al., 2016) and included thermal properties such as specific heat capacity (1.70 J g^{-1} ºC^{-1}) and thermal conductivity (0.065 W m^{-1} ºC^{-1}), as well as microbial growth-related parameters: heat yield from growth, activation energies E_{A1} (70225 J mol^{-1}) and E_{A2} (283356 J mol^{-1}), and the pre-exponential factors A (2.69 ×10^7 s^{-1}) and B (1.30 ×10^{47}) used in the temperature-dependence growth equation. The experimental value for the specific growth rate was retained. As observed above, the results clearly demonstrate that the model using

experimental parameters provides a significantly better fit to the experimental data, particularly in predicting both the magnitude and timing of the temperature peak. While the simulation based on bibliographic parameters captures the general trend, it underestimates the maximum temperature and exhibits an earlier decline than observed experimentally. This discrepancy highlights the importance of parameter determination under specific experimental conditions, especially in SSF processes, where heat generation is closely tied to microbial metabolic activity and system-specific factors such as porosity, moisture content, and heat transfer.

On the other hand, all parameters related to microbial kinetics—including the heat yield associated with growth—must be determined experimentally for each SSF system. Even when literature values originate from the same microorganism, the physiological differences between SmF and SSF can render them unsuitable. Our sensitivity analysis confirms that such discrepancies result in high norm values, which preclude their direct application. Consequently, relying on kinetic data from other strains or processes is not a viable strategy. A thorough experimental characterisation of microbial kinetics is therefore essential prior to modelling, as these parameters have the strongest impact on the predicted solid temperature and are the most sensitive components of the model.

4. Conclusions

This study proposes and implements a comprehensive methodology for the determination of critical parameters for the mathematical modelling of solid-state fermentation systems. Focusing on SL production using *S. bombicola*, the methodology integrates experimental determination of microbial kinetics, thermal properties, and transfer coefficients into a two-phase model. The experimentally determined values were: specific heat capacity of 1.55 J g^{-1} °C^{-1}, thermal conductivity of 0.127 W m^{-1} °C^{-1}, heat transfer coefficient of 9790 ± 2.25 W m^{-3} °C^{-1}, mass transfer coefficient 0.00189 ± 0.00078 s^{-1}, metabolic heat yield of 1.34 × 10^7 J kg^{-1} biomass and a specific growth rate of 0.389 h^{-1}.The model accurately predicts the temperature profile in a 22-L bioreactor, and the sensitivity analysis highlights the strong influence of microbial growth parameters and heat yield on model performance. In contrast, parameters such as specific heat capacity, thermal conductivity, and mass and heat transfer coefficients showed limited impact and may be estimated from literature when appropriately selected. In addition, when literature-based parameters were used, the resulting temperature profile showed lower agreement with experimental data. In contrast, employing experimentally determined parameters provided a closer approximation to the experimental temperature profile, highlighting the relevance of using specific values to improve accuracy. This dual outcome — a robust methodology and specific values for SSF-based SL production — provides a valuable tool for future model-based scale-up and optimization of similar SSF processes.

CRediT authorship contribution statement

Albert Guisasola: Writing – review & editing, Validation, Supervision, Software. **Carrasco-Garcia Anna:** Writing – original draft, Visualization, Validation, Software, Methodology, Investigation, Formal analysis, Data curation. **Teresa Gea:** Writing – review & editing, Supervision, Project administration, Funding acquisition, Formal analysis, Conceptualization. **Moral Vico Javier:** Writing – review & editing, Validation, Supervision, Formal analysis.

Declaration of Competing Interest

The authors declare the following financial interests/personal relationships which may be considered as potential competing interests: Teresa Gea reports financial support was provided by Spain Ministry of Science and Innovation. If there are other authors, they declare that they have no known competing financial interests or personal relationships that could have appeared to influence the work reported in this paper.

Acknowledgements

This research was financially supported by the Spanish Ministerio de Ciencia e Innovación (Project SOLSTICE, PID2023–146978OB-100). Anna Carrasco García thanks UAB for the PIF scholarship granted for the completion of her PhD thesis.

Appendix A. Supporting information

Supplementary data associated with this article can be found in the online version at doi:10.1016/j.cherd.2026.03.024.

References

Raghavarao, K.S.M.S., Ranganathan, T.V., Karanth, N.G., 2003. Some engineering aspects of solid-state fermentation. Biochem. Eng. J. 13 (2–3), 127–135. https://doi.org/10.1016/S1369-703X(02)00125-0.

Finkler, A.T.J., De Lima Luz, L.F., Krieger, N., Mitchell, D.A., Jorge, L.M., 2021. A model-based strategy for scaling-up traditional packed-bed bioreactors for solid-state fermentation based on measurement of O2 uptake rates. Biochem. Eng. J. 166, 107854. https://doi.org/10.1016/j.bej.2020.107854.

Kumar, V., Ahluwalia, V., Saran, S., Kumar, J., Patel, A.K., Singhania, R.R., 2021. Recent developments on solid-state fermentation for production of microbial secondary metabolites: challenges and solutions. Bioresour. Technol. 323, 124566. https://doi.org/10.1016/j.biortech.2020.124566.

Sánchez, A., et al., 2024. Solid-state fermentation: a review of its opportunities and challenges in the framework of circular bioeconomy. Afinidad J. Chem. Eng. Theor. Appl. Chem. 81 (601), 51–57. https://doi.org/10.55815/424209.

Arora, S., Rani, R., Ghosh, S., 2018. Bioreactors in solid state fermentation technology: design, applications and engineering aspects. J. Biotechnol. 269, 16–34. https://doi.org/10.1016/j.jbiotec.2018.01.010.

Hamidi-Esfahani, Z., Shojaosadati, S.A., Rinzema, A., 2004. Modelling of simultaneous effect of moisture and temperature on A. niger growth in solid-state fermentation. Biochem. Eng. J. 21 (3), 265–272. https://doi.org/10.1016/j.bej.2004.07.007.

Casciatori, F.P., Bück, A., Thoméo, J.C., Tsotsas, E., 2016. Two-phase and two-dimensional model describing heat and water transfer during solid-state fermentation within a packed-bed bioreactor. Chem. Eng. J. 287, 103–116. https://doi.org/10.1016/j.cej.2015.10.108.

Ashley, V.M., Mitchell, D.A., Howes, T., 1999. Evaluating strategies for overcoming overheating problems during solid-state fermentation in packed bed bioreactors. Biochem. Eng. J. 3 (2), 141–150. https://doi.org/10.1016/S1369-703X(99)00010-8.

Mitchell, D.A., 2006. Solid state fermentation bioreactors: fundamentals of design and operation; with 32 tables. Springer, Berlin Heidelberg.

Yang, L., et al., 2025. Machine learning combined with GC-FID for discrimination of different categories of maotai-flavor baijiu. Food Chem. X 28, 102555. https://doi.org/10.1016/j.fochx.2025.102555.

Amenaghawon, A.N., et al., 2024. Surfactant-facilitated metabolic induction enhances lipase production from an optimally formulated waste-derived substrate mix using Aspergillus niger: A case of machine learning modeling and metaheuristic optimization. Bioresour. Technol. Rep. 28, 101993. https://doi.org/10.1016/j.biteb.2024.101993.

Mitchell, D.A., Ruiz, H.A., Krieger, N., 2023. A critical evaluation of recent studies on packed-bed bioreactors for solid-state fermentation. Processes 11 (3), 872. https://doi.org/10.3390/pr11030872.

Casciatori, F.P., Laurentino, C.L., Magdaleno Lopes, K.C., Gonçalves De Souza, A., Thoméo, J.C., 2013. Stagnant effective thermal conductivity of agro-industrial residues for solid-state fermentation. Int. J. Food Prop. 16 (7), 1578–1593. https://doi.org/10.1080/10942912.2011.603171.

Zhang, Y., Wang, L., Chen, H., 2017. Correlations of medium physical properties and process performance in solid-state fermentation. Chem. Eng. Sci. 165, 65–73. https://doi.org/10.1016/j.ces.2017.02.039.

Casciatori, F.P., Laurentino, C.L., Taboga, S.R., Casciatori, P.A., Thoméo, J.C., 2014. Structural properties of beds packed with agro-industrial solid by-products applicable for solid-state fermentation: Experimental data and effects on process performance. Chem. Eng. J. 255, 214–224. https://doi.org/10.1016/j.cej.2014.06.040.

Von Meien, O.F., Mitchell, D.A., 2002. A two-phase model for water and heat transfer within an intermittently-mixed solid-state fermentation bioreactor with forced aeration. Biotechnol. Bioeng. 79 (4), 416–428. https://doi.org/10.1002/bit.10268.

Finkler, A.T.J., et al., 2021. Estimation of heat and mass transfer coefficients in a pilot packed-bed solid-state fermentation bioreactor. Chem. Eng. J. 408, 127246. https://doi.org/10.1016/j.cej.2020.127246.

Maddikeri, G.L., Gogate, P.R., Pandit, A.B., 2015. Improved synthesis of sophorolipids from waste cooking oil using fed batch approach in the presence of ultrasound. Chem. Eng. J. 263, 479–487. https://doi.org/10.1016/j.cej.2014.11.010.

Scotti, C.T., Vergoignan, C., Feron, G., Durand, A., 2001. Glucosamine measurement as indirect method for biomass estimation of Cunninghamella elegans grown in solid

state cultivation conditions. Biochem. Eng. J. 7 (1), 1–5. https://doi.org/10.1016/S1369-703X(00)00090-5.
Abd-Aziz, S., Hung, G.S., Hassan, M.A., Abdul Kari, M.I., Samat, N., 2008. Indirect method for quantification of cell biomass during solid-state fermentation of palm kernel cake based on protein content. Asian J. Sci. Res. 1 (4), 385–393. https://doi.org/10.3923/ajsr.2008.385.393.
Nout, M.J.R., Bonants-van Laarhoven, T.M.G., De Jongh, P., De Koster, P.G., 1987. Ergosterol content of Rhizopus oligosporus NRRL 5905 grown in liquid and solid substrates. Appl. Microbiol. Biotechnol. 26 (5), 456–461. https://doi.org/10.1007/BF00253532.
Rodríguez-Rodríguez, C.E., Marco-Urrea, E., Caminal, G., 2010. Degradation of naproxen and carbamazepine in spiked sludge by slurry and solid-phase Trametes versicolor systems. Bioresour. Technol. 101 (7), 2259–2266. https://doi.org/10.1016/j.biortech.2009.11.089.
Feng, X.M., Eriksson, A.R.B., Schnürer, J., 2005. Growth of lactic acid bacteria and Rhizopus oligosporus during barley tempeh fermentation. Int. J. Food Microbiol. 104 (3), 249–256. https://doi.org/10.1016/j.ijfoodmicro.2005.03.005.
Córdova-López, J., Gutiérrez-Rojas, M., Huerta, S., Saucedo-Castañeda, G., Favela-Torres, E., 1996. 'Biomass estimation of Aspergillus niger growing on real and model supports in solid state fermentation'. Biotechnol. Tech. 10 (1), 1–6. https://doi.org/10.1007/BF00161075.
Favela-Torres, E., Cordova-López, J., García-Rivero, M., Gutiérrez-Rojas, M., 1998. Kinetics of growth of Aspergillus niger during submerged, agar surface and solid state fermentations. Process Biochem. 33 (2), 103–107. https://doi.org/10.1016/S0032-9592(97)00032-0.
Rodríguez, A., Gea, T., Font, X., 2021. Sophorolipids production from oil cake by solid-state fermentation. Inventory for economic and environmental assessment. Front. Chem. Eng. 3, 632752. https://doi.org/10.3389/fceng.2021.632752.
Oiza, N., Moral-Vico, J., Sánchez, A., Gea, T., 2024. Enhanced anaerobic digestion of food waste using purified lactonic sophorolipids produced by solid-state fermentation of molasses and oil waste: A circular approach. J. Clean. Prod. 468, 143062. https://doi.org/10.1016/j.jclepro.2024.143062.
Eras-Muñoz, E., Font, X., Gea, T., 2024. A comparative study of oilseed cakes as hydrophobic feedstocks for sophorolipid production by solid-state fermentation. Ind. Crops Prod. 222, 120059. https://doi.org/10.1016/j.indcrop.2024.120059.
Mejias, L., Ruiz, D., Molina-Peñate, E., Barrena, R., Gea, T., 2025. Bacillus thuringiensis derived biopesticides from biowaste digestate at 290-L demonstration scale through solid-state fermentation. Environ. Technol. Innov. 37, 103974. https://doi.org/10.1016/j.eti.2024.103974.
Pitol, L.O., Biz, A., Mallmann, E., Krieger, N., Mitchell, D.A., 2016. Production of pectinases by solid-state fermentation in a pilot-scale packed-bed bioreactor. Chem. Eng. J. 283, 1009–1018. https://doi.org/10.1016/j.cej.2015.08.046.
Jiménez-Peñalver, P., Gea, T., Sánchez, A., Font, X., 2016. Production of sophorolipids from winterization oil cake by solid-state fermentation: optimization, monitoring and effect of mixing. Biochem. Eng. J. 115, 93–100. https://doi.org/10.1016/j.bej.2016.08.006.
Rodríguez, A., Gea, T., Sánchez, A., Font, X., 2021. Agro-wastes and inert materials as supports for the production of biosurfactants by solid-state fermentation. Waste Biomass.. Valoriz. 12 (4), 1963–1976. https://doi.org/10.1007/s12649-020-01148-5.
Cooney, C.L., Wang, D.I.C., Mateles, R.I., 1968. Measurement of heat evolution and correlation with oxygen consumption during microbial growth. Biotechnol. Bioeng. 67 (6), 691–703. https://doi.org/10.1002/(SICI)1097-0290(20000320)67:6<691::AID-BIT7>3.0.CO;2-R.
D.F.O. James E. Bailey, Biochemical Engineering Fundamentals.
Ruggieri, L., Gea, T., Artola, A., Sánchez, A., 2009. Air filled porosity measurements by air pycnometry in the composting process: a review and a correlation analysis. Bioresour. Technol. 100 (10), 2655–2666. https://doi.org/10.1016/j.biortech.2008.12.049.
Jin, G., Zhu, Y., Xu, Y., 2017. Mystery behind Chinese liquor fermentation. Trends Food Sci. Technol. 63, 18–28. https://doi.org/10.1016/j.tifs.2017.02.016.
Koh, C.H., Gauvin, F., Schollbach, K., Brouwers, H.J.H., 2023. Upcycling wheat and barley straws into sustainable thermal insulation: assessment and treatment for durability. Resour. Conserv. Recycl 198, 107161. https://doi.org/10.1016/j.resconrec.2023.107161.
Tansel, B., 2023. Thermal properties of municipal solid waste components and their relative significance for heat retention, conduction, and thermal diffusion in landfills. J. Environ. Manag. 325, 116651. https://doi.org/10.1016/j.jenvman.2022.116651.
Vauris, A., Valcauda, S., Husson, F., Coninck, J.D., 2022. A novel method to assess heat transfer and impact of relevant physicochemical parameters for the scaling up of solid state fermentation systems. Biotechnol. Rep. 36, e00764. https://doi.org/10.1016/j.btre.2022.e00764.
Khanahmadi, M., Roostaazad, R., Bozorgmehri, R., Safekordi, A., 2005. Thermal conductivity of moist wheat bran beds used in solid state fermentations. Food Bioprod. Process 83 (3), 185–190. https://doi.org/10.1205/fbp.04043.
Teresa, Gea, et al., 2024. Unlocking the potential of solid-state fermentation with insights into organic waste selection and thermal dynamics for sustainable sophorolipids production. Chem. Eng. Trans. 109, 409–414. https://doi.org/10.3303/CET24109069.
Abdul Manan, M., Webb, C., 2018. Estimation of growth in solid state fermentation: a review. Malays. J. Microbiol. https://doi.org/10.21161/mjm.96616.
Mille-Lindblom, C., Von Wachenfeldt, E., Tranvik, L.J., 2004. Ergosterol as a measure of living fungal biomass: persistence in environmental samples after fungal death. J. Microbiol. Methods 59 (2), 253–262. https://doi.org/10.1016/j.mimet.2004.07.010.
Hirayama, T., et al., 2020. ERG3-Encoding Sterol C5,6-DESATURASE in Candida albicans is required for virulence in an enterically infected invasive Candidiasis mouse model. Pathogens 10 (1), 23. https://doi.org/10.3390/pathogens10010023.
Vella, F.M., Calandrelli, R., Del Barone, A., Guida, M., Laratta, B., 2023. Rapid evaluation of ergosterol to detect yeast contamination in fruit juices. Eur. Food Res. Technol. 249 (2), 465–472. https://doi.org/10.1007/s00217-022-04145-1.
Pasanen, A.-L., Yli-Pietilä, K., Pasanen, P., Kalliokoski, P., Tarhanen, J., 1999. Ergosterol content in various fungal species and biocontaminated building materials. Appl. Environ. Microbiol 65 (1), 138–142. https://doi.org/10.1128/AEM.65.1.138-142.1999.
García-Ochoa, F., Casas, J.A., 1999. Unstructured kinetic model for sophorolipid production by Candida bombicola. Enzym. Microb. Technol. 25 (7), 613–621. https://doi.org/10.1016/S0141-0229(99)00089-7.
Mitchell, D.A., Von Meien, O.F., Krieger, N., Dalsenter, F.D.H., 2004. A review of recent developments in modeling of microbial growth kinetics and intraparticle phenomena in solid-state fermentation. Biochem. Eng. J. 17 (1), 15–26. https://doi.org/10.1016/S1369-703X(03)00120-7.
Vedaraman, N., Venkatesh, N., 2010. The effect of medium composition on the production of sophorolipids and the tensiometric properties by Starmerella bombicola MTCC 1910. PJCT 12 (2), 9–13. https://doi.org/10.2478/v10026-010-0011-4.
Sargantanis, J., Karim, M.N., Murphy, V.G., Ryoo, D., Tengerdy, R.P., 1993. Effect of operating conditions on solid substrate fermentation. Biotechnol. Bioeng. 42 (2), 149–158. https://doi.org/10.1002/bit.260420202.
Ribeiro, I.A., Bronze, M.R., Castro, M.F., Ribeiro, M.H.L., 2013. Sophorolipids: improvement of the selective production by Starmerella bombicola through the design of nutritional requirements. Appl. Microbiol. Biotechnol. 97 (5), 1875–1887. https://doi.org/10.1007/s00253-012-4437-x.
Rahardjo, Y.S.P., Tramper, J., Rinzema, A., 2006. Modeling conversion and transport phenomena in solid-state fermentation: a review and perspectives. Biotechnol. Adv. 24 (2), 161–179. https://doi.org/10.1016/j.biotechadv.2005.09.002.
Celligoi, M.A.P.C., Silveira, V.A.I., Hipólito, A., Caretta, T.O., Baldo, C., 2020. Sophorolipids: a review on production and perspectives of application in agriculture. Span. J. Agric. Res. 18 (3), e03R01. https://doi.org/10.5424/sjar/2020183-15225.
V.J. Parekh, V.B. Patravale, and A.B. Pandit, 'Mango kernel fat: A novel lipid source for the fermentative production of sophorolipid biosurfactant using Starmerella Bombicola NRRL-Y 17069', 2012.
Felse, P.A., Shah, V., Chan, J., Rao, K.J., Gross, R.A., 2007. Sophorolipid biosynthesis by Candida bombicola from industrial fatty acid residues. Enzym. Microb. Technol. 40 (2), 316–323. https://doi.org/10.1016/j.enzmictec.2006.04.013.
Rodrigues, N.A., Katayama, E.T., Casciatori, F.P., 2022. Alternative strategies to perform solid-state cultivation in a multilayer packed-bed bioreactor: continuous and cyclic operations. Chem. Eng. J. 448, 137726. https://doi.org/10.1016/j.cej.2022.137726.
Sangsurasak, P., Mitchell, D.A., 1998. Validation of a model describing two-dimensional heat transfer during solid-state fermentation in packed bed bioreactors. Biotechnol. Bioeng. 60 (6), 739–749. https://doi.org/10.1002/(SICI)1097-0290(19981220)60:6<739::AID-BIT10>3.0.CO;2-U.